HAL open science

Hydrothermal simulation in a fault zone: Impact and efficiency of different stimulation methods

Antoine Armandine Les Landes, Julie Maury, Théophile Guillon, Simon Lopez, Arnold Blaisonneau, van Hieu Tran, Annick Loschetter, Mariane Peter-Borie

To cite this version:

Antoine Armandine Les Landes, Julie Maury, Théophile Guillon, Simon Lopez, Arnold Blaisonneau, et al.. Hydrothermal simulation in a fault zone: Impact and efficiency of different stimulation methods. 2019. hal-02391397

HAL Id: hal-02391397

https://brgm.hal.science/hal-02391397v1

Preprint submitted on 3 Dec 2019

HAL is a multi-disciplinary open access archive for the deposit and dissemination of scientific research documents, whether they are published or not. The documents may come from teaching and research institutions in France or abroad, or from public or private research centers.

L'archive ouverte pluridisciplinaire **HAL**, est destinée au dépôt et à la diffusion de documents scientifiques de niveau recherche, publiés ou non, émanant des établissements d'enseignement et de recherche français ou étrangers, des laboratoires publics ou privés.

Proceedings World Geothermal Congress 2020
Reykjavik, Iceland, April 26 – May 2, 2020

Hydrothermal simulation in a fault zone: Impact and efficiency of different stimulation methods

Antoine ARMANDINELESLANDES, Julie MAURY, Théophile GUILLON, Simon LOPEZ, Arnold BLAISONNEAU, Van Hieu TRAN, Annick LOSCHETTER and Mariane PETER-BORIE

BRGM, 3 Avenue Claude Guillemin, 45100 Orléans, FRANCE

a.armandineleslandes@brgm.fr

Keywords: fluid flow, heat transfer, stimulation, scenarios, fault, geothermal, numerical modeling, DEEPEGS

ABSTRACT

The H2020-DEEPEGS project aims to demonstrate the feasibility of the Enhanced/Engineered Geothermal System Technology (EGS) to produce electricity and/or heat. One of the main technological challenges is to optimise the well architecture and stimulation methods to get economically viable flow rate in deep hot reservoir initially little productive (Peter-borie et al., 2020). The main idea of this work is to provide an overview of the impact of different stimulation methods considered to enhance the productivity of the targeted reservoir of an EGS demonstrator. The targeted fault zone is located in the granitic basement of the Upper Rhine Graben (Eastern France), at around 4400m TVD (True Vertical Depth) where the temperature is estimated around 200°C. Based on the drilling data recorded and structural hypothesis hinging on a multiscale approach, a conceptual model of the faulted geothermal reservoir is established. Then, a hydrothermal model of the fault zone is built. The numerical model is developed using the ComPASS code that enables the implementation of 2D discrete fracture or fault network coupled with the surrounding 3D matrix (so-called hybrid-dimensional model). The current code is able to handle compositional multiphase Darcy flows, relying on a Coats type formulation, coupled to the conductive and convective transfers of energy (Lopez et al., 2018). The impact of the different technologies used to enhance the injectivity of the well such as stimulation methods (the hydraulic and thermal stimulations are considered) or such as a multi-drain well geometry are studied through the simulation of an injection test. The effect of soft hydraulic stimulation resulting from the hydromechanical simulations (Blaisonneau et al., 2020a) is implemented into the hydrothermal model through the modification of the fractured reservoir properties. In parallel based on the same hydrothermal model the impact of multi-drain well geometry is studied. For each stimulation method, the injectivity can be compared with the initial model and the relative efficiency of each stimulation method can be assessed. Based on the knowledge of temperature fields obtained for each case through the hydrothermal simulations and using the results provided by the thermomechanical models (Peter-Borie et al., 2019), the permeability variations (around the well and in the matrix surrounding the fractures) are implemented into the hydrothermal model in order to assess the impact of thermal stimulation. The main aim of this study is to assess the influence of different stimulation methods into a unique hydrothermal model in order to test different stimulation scenarios. The final goal of this work is to provide numerical tools in order to investigate the relative efficiency of stimulation methods in the context of EGS.

1. INTRODUCTION

In some contexts, it is often not possible to extract the Earth's thermal energy under economic conditions without implementing technological solutions (so called "Enhanced/Engineered Geothermal System", abbreviated EGS) to increase the injectivity/productivity of the wells. To be able to generalize the exploitation of deep geothermal energy, these cases must be addressed through appropriate technological solutions. The H2020-DEEPEGS project (grant agreement No 690771) aims at demonstrating the feasibility of EGS for delivering energy from renewable resources in Europe. In this framework, two deep geothermal wells in Iceland and in France were drilled to demonstrate the EGS technology in different geological contexts (Peter-borie et al., 2020).

In France, the Vendenheim (VDH) doublet is located in the Upper Rhine Graben (URG), in Eastern France. The target is a fault zone in the granitic basement. The reached temperature at around 4400 m TVD is estimated around 200°C. The initial injectivity/productivity index, is far from the economically viable target. Under such conditions, several operations are considered to enhance the output of the wells, either by improving near-well permeability, or by opening hydrological connections to permeable zones not directly intersected by the well. The methods generally used are based on the activation of mechanical, thermal and/or chemical mechanisms that drive to rock permeability enhancement as well as multi-drain well geometry (see Peter-borie et al., 2020 for a detailed description concerning the stimulation methods and the context of this study).

Within the H2020-DEEPEGS project, in order to study the impact of stimulation scenarios on the permeability development, we assess different stimulation methods and well architectures for both demonstrators by numerical modelling. This paper aims to assess the relative impact of several technologies for the VDH demonstrator using a hydrothermal model and based on the results of hydromechanical and thermomechanical models presented in companion papers (Blaisonneau et al., 2020; Peter-Borie et al., 2019).

2. CONCEPTUAL MODEL OF VENDENHEIM RESERVOIR

The VDH demonstrator is located in the URG, which is part of the European Cenozoic Rift System (ECRIS, Ziegler, 1990 among many others). This approximately 300 km-long and 40 km-wide rift is bounded on the French side by the Vosges Mountains and on the German side by the Black Forest (Figure 1).

The VDH demonstrator targets a N10°E-striking and 82°W-dipping fault in the plutonic basement in the North of Strasbourg. Based on the tectonic history (polyphasic tectonic) of the Rhine graben and the orientation of the main faults surrounding the target fault of the VDH demonstrator, it can be assumed that this target fault in the basement has been formed by a sinistral shearing during the Paleozoic and reactivated during Cenozoic Times (Edel et al., 2007; Schumacher, 2002, among others). A conceptual model of the

fault zone is proposed in Figure 1 (Peter-borie et al., 2020); it is based on drilling data and cutting analyses. Here are recalled some of the main characteristics (especially those related to hydraulic features) of this model. In the basement, based on the identified losses, the fault zone can be distinguished in three main zones (see Figure 1 where blue stars correspond to losses):

(1) A damage zone in the upper part of the openhole with one main loss at the top of the damage zone and then several minor losses distributed along the damage zone

(2) A sealed fault core with a low permeability (with no losses)

(3) A transmissive fault core (heavily fractured zone: cataclasite) with diffuse losses. Note that Euhedral quartz has been found in the cuttings, probably linked to hydrothermal sealing of discontinuities.

From a hydraulic point of view, the major interfaces that delineate the three main zones of this fault zone appear favorable to flow. Firstly, the major loss is located at the top of the damage zone. Then, two anomalies of chlorite crystallization temperature are localized between the two fault cores or at the interface between altered and moderately altered zones. These anomalies characterize preferential circulations. These observations are in agreement with in-situ measurements of Rittershoffen wells where interfaces are considered as the major circulation zones (Glaas et al., 2018).

Little data is available with respect to hydrogeological functioning of the reservoir. Due to the lack of information and based on measurements from the Cronenbourg wells (few km from the study area), a hydrostatic state is considered, where a pressure of approximately 279 bars is measured at a depth of 2755 m (Cruz Mermy et al., 2012). Note that in its upper part (above the basement), the target fault intersects some permeable units at many depths, which can act as a reservoir. For the final measured depth of wells, around 4400 m TVD the temperature estimated is around 200°C and the salinity of the fluid within the reservoir is estimated around 100 g/L. If a hydrostatic state is assumed for the reservoir, a pressure of 431 bars at a depth of 4290 m is expected. This pressure value is in accordance with other wells pressure measured in the same hydrogeological context (Rittershoffen, Soultz-sous-Forêts).

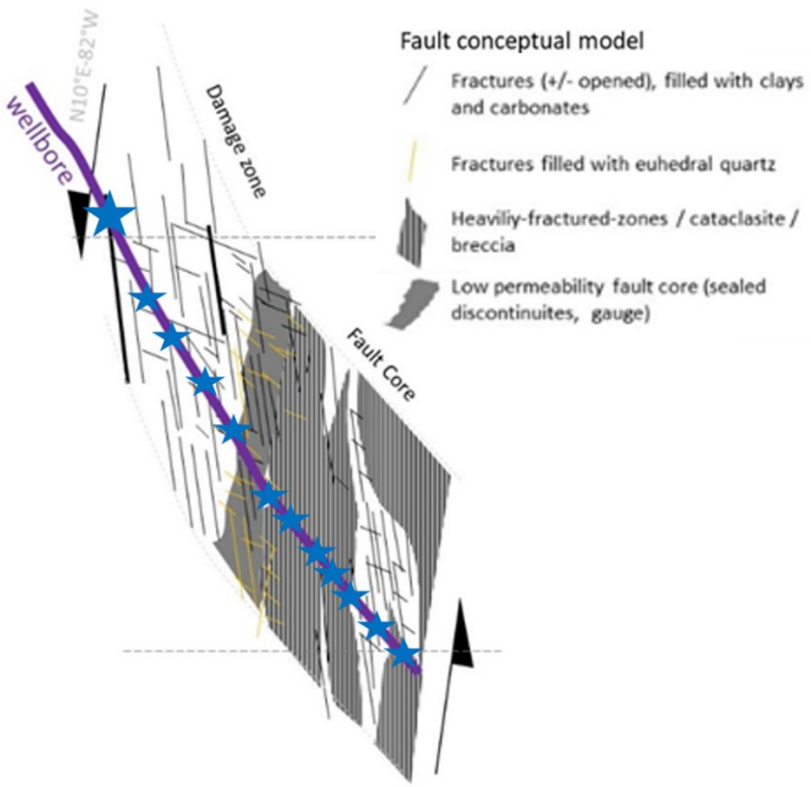

Figure 1: Conceptual model of the geometry of the targeted fault zone based on the drilling data (modified from Peter-Borie et al. 2020). Blue stars correspond to losses.

Based on these first observations, we can notice that the major loss is located at the top of the damage zone and then several minor losses are distributed along the damage zone until to the sealed fault core. This distribution of losses is not a feature of a decreasing of permeability (fracture density) with the distance to the fault core. Then, the structural organization of the fault zone is very heterogeneous. Moreover, data issued from previous studies, such as Soultz-sous-Forêts or more recently Rittershoffen (Baujard et al., 2017) demonstrate that the hydraulic behavior of this reservoir is controlled by discontinuous structures at pluri-hectometric scale with multiple orientations related to the orientation of the Euclidian structures and the nature of the fault (formation context). On this basis (considering these discontinuous structures), the functioning of the fractured reservoir can be explained (see Gentier et al., 2014). Considering the importance of discrete fractures, it appears appropriate and relevant to consider discrete element methods to assess and understand this kind of reservoir.

Here, as previously mentioned, borehole data to identify fracture orientations are not available. To overcome this lack of information and go further in the understanding of the flow paths around the well during stimulation methods, a Discrete Fracture Network (DFN) is built based on the assumptions that: i. the URG is globally an Andersonian system; ii. the fault has been formed by a sinistral shearing. Rocks which are sheared by brittle or cataclastic processes often develop a characteristic structural pattern of fractures (Cloos, 1928; Katz et al., 2004; Riedel, 1929) and then can serve as basis to develop a theoretical geometry of the subfracturing. Then

using this generic concept to conceptualize the subfracturing (Figure 2, Riedel fracture sets) of the fault zone, a DFN is built for the N10°E-striking and 82°W-dipping fault.

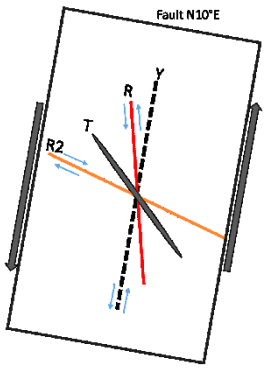

Figure 2. Riedel concept: Fractures classically developed in shear zones with blue and gray arrows are the sense of shear. R: Riedel shears which are normally the first subsidiary fractures to occur. R2 shears are antithetic fractures, conjugate with R shears. Y shears are synthetic fractures subparallel to the main fault. T are theoretical distribution of tensional fractures.

3. NUMERICAL MODEL

3.1 Numerical codes

The 3D numerical model is constructed using three successive different codes.

3.1.1 3DEC

Firstly, we used the 3DEC software (which is based on the Distinct Element Method (3DEC TM)) to generate the DFN. The 3DEC software will be used to simulate the hydromechanical stimulation (see Blaisonneau et al., 2020a for more details). The same geometry will be used for the hydromechanical and thermohydraulic models in order to facilitate the exchanges. The building step of the geometry is described in section 3.2 Geometry below.

3.1.2 SALOME

The open-source software platform named SALOME is used to rebuild the same geometry (resulting from the mechanical model) and to mesh the whole domain, in order to, ultimately, simulate hydrothermal flows in the fault zone using the ComPASS platform. The platform is available under Lesser General Public License (LGPL) at http://www.salome-platform.org. SALOME is actively developed with the support of Open CASCADE. SALOME results from a collaborative development approach between the CEA and EDF. SALOME uses two languages, Python and C++. The main functionalities of these parts are accessible by scripting languages and/or the graphical user interface. The platform also takes distributed meshes into account, thus facilitating parallel computations (Ribés et al., 2017).

3.1.1 ComPASS

This part describes briefly the ComPASS platform (its main components and characteristics). The reader interested in further details is referred to the works of Xing et al., (2017) for the description of the theoretical and numerical aspects of the modeling of compositional multiphase flows in fractured media, Beaude et al.,(2017) for the integration of complex well architectures (Beaude et al., 2017b) and the specification of complex boundary conditions (Beaude et al., 2018). Additional information is also available on http://www.anr-charms.org and in Lopez et al., (2018).

The continuous multiphase multicomponent model

The ComPASS code is based on a Coats type formulation (Coats, 1989) which extends the work by Eymard et al. (2012) to non-isothermal flows. It accounts for an arbitrary nonzero number of components in each phase allowing to model immiscible, partially miscible or fully miscible flows. The number of phases and number of components are hard-coded for each thermodynamical module. As the model takes into account phase change reactions which are assumed to be at equilibrium, phases can appear or disappear. Thermodynamical properties of each phase depend on the phase pressures, the temperature, and the phase molar fractions. These properties are specified by the user as hard coded functions along with their derivatives. The reader interested in further details is referred to the paper of Lopez et al. (2018) and references therein for the description of the theoretical and numerical aspects of the modeling of compositional multiphase flows in fractured media.

Hybrid model including a discrete fracture network

Two classes of models, dual continuum and discrete fracture models, are typically employed and possibly coupled to simulate flow and transport in fractured porous media. Discrete fracture models (DFM) represent explicitly the fractures as codimension one surface immersed in the surrounding matrix domain. ComPASS uses the DFM approach with a lower dimension physical model along the fracture which is derived from the equi-dimensional model of the previous paragraph by integration and averaging along the – possibly variable - width of each fracture. The resulting so-called hybrid-dimensional model couples the 3D model in the matrix with a 2D model in the fracture network taking into account the jump of the normal fluxes as well as additional transmission conditions at the matrix fracture interfaces. These transmission conditions depend on the mathematical nature of the equi-dimensional model and on additional physical assumptions depending on the fracture behavior (drain vs. barrier). The interested reader is referred to the paper by Xing et al. (2017) for further details.

Wells integration

A first version of reservoir well interaction has been implemented into the ComPASS platform and validated for monophasic cases (Beaude et al., 2017a). The well is modeled as a Dirac source term along the well trajectory. Most well models in reservoir simulations are defined by a set of connected perforations, each perforation belonging to a cell of the mesh (e.g. source block in TOUGH2). In order to take advantage of unstructured meshes and of the nodal feature of the Vertex Approximate Gradient VAG scheme, it is more convenient in our case to discretize each well as a subset of edges of the mesh. This alternative approach provides an efficient way to represent slanted and multi-branches wells. The fluxes connecting the well with the 3D matrix and the 2D fracture network at each node of the well are computed using Peaceman's approach (Chen and Zhang, 2009; Peaceman, 1983, 1978). It is based on a Two Point Flux Approximation (TPFA) with a transmissibility taking into account the unresolved singularity of the pressure (or temperature) solution in the neighborhood of the well. The non-isothermal flow model inside the well is defined using a single implicit unknown for each well corresponding to a reference pressure often coined as the bottom hole pressure. The pressures along the well are then deduced from this bottom hole pressure with the crude assumption that the pressure is hydrostatic inside the well. The temperatures along the well are computed assuming thermal equilibrium and a stationary flow inside the well.

3.2 Geometry

The domain is chosen large enough to enable hydrothermal simulation and integrate the size of major discontinuous elements. The numerical model domain is a block of rock measuring 500 m in the x- y- and z-directions and centered on the open-hole of the well. This domain is delineated with four major discontinuities (DZup, DZdown_FC1up, FC1down_FC2up and FC2down, see Figure 3a) that correspond to four major interfaces, which can be considered as the major circulation zones. These major discontinuities are used to delineate major zones (subdomains): the Damage Zone (DZ), the Sealed Fault Core (FC1), the Transmissive Fault Core (FC2) and the surrounding impermeable matrix (Figure 3b).

The second step is to generate a conceptual DFN in accordance with the number of productive fractures that intersect the well along the fault. Prior to fracture generation, a domain must be specified. Here, the generation volume is constrained by the two major discontinuities that delineate the DZ zone. Three fracture sets are defined and generated in separate steps. For each set, the DFN is defined according to the size and orientation distributions. Then fractures are generated until the target fracture frequency (number of fractures intersecting the well: P10) is reached. Here, we consider the number of intersections with the well in the DZ. We do this because the DZ has the more distributed losses, we consider the FC1 is only involved peripherally in the circulation and the FC2 is heavily permeable so a unique structure is enough to model it. Three families are considered (Table 1): R, R2 and Y (DZup, DZDown_FC1up, FC1down_FC2up, FC2down) according to the Riedel concept (Figure 3c).

Table 1. Fracture set properties

Fracture set	Property	Distribution	Parameters
R	positions orientations lengths density	Uniform Uniform Power law	Positions generated in all DZ space Dip: 82.48°, Dip direction 259.82° Scaling exponent: a = 2, lmin = 20, lmax = 200 P10
R2	positions orientations lengths density	Uniform Uniform Power law	Positions generated in all DZ space Dip: 87.27°, Dip direction 209.82° Scaling exponent: a = 2, lmin = 20, lmax = 200 P10
Y	positions orientations lengths	Deterministic	Interfaces Dip: 82.24°, Dip direction 280° 500m

In order to perform the hydromechanical simulations, the DFN has been simplified. First, fractures can be isolated, disconnected from the largest cluster (here we assumed that the largest cluster is connected to the well). Then, isolated fractures are deleted. A second simplification is achieved by combining fractures that are too close together and subparallel (in our case when they belong to the same family). Here for each set (R and R2) the smaller fractures are deleted and replaced by a larger fracture when the normal distance with one other fracture is less than 23 m. Note that the area of the larger fracture is increased in accordance with the size of the deleted ones. Thus, some properties of the DFN are modified. The resulting DFN is shown in Figure 3d. The last simplification of the DFN corresponds to the deletion of dead-end of fractures (above the DZup and below the FC1down_FC2up limits). The following step is to build the geometry, introduce the DFN into the 3D domain (Figure 3e and Figure 3f) and then mesh the model (tetrahedral conformal meshing) using the SALOME code (Figure 3g). The final mesh is composed of more than 183 000 nodes and more than 1 billion of elements. Note that this geometry is implemented in the hydromechanical and hydrothermal models. To be consistent with the conceptual model, the permeable fault core (FC2) will be an equivalent porous media (permeable) and the impermeable fault core (FC1) will be fractured (surrounded by an impermeable porous media) as a prolongation of the fractures within the DZ. The fractures through the FC1 zone allow a possible connection between the DZ zone and the FC2 permeable zone.

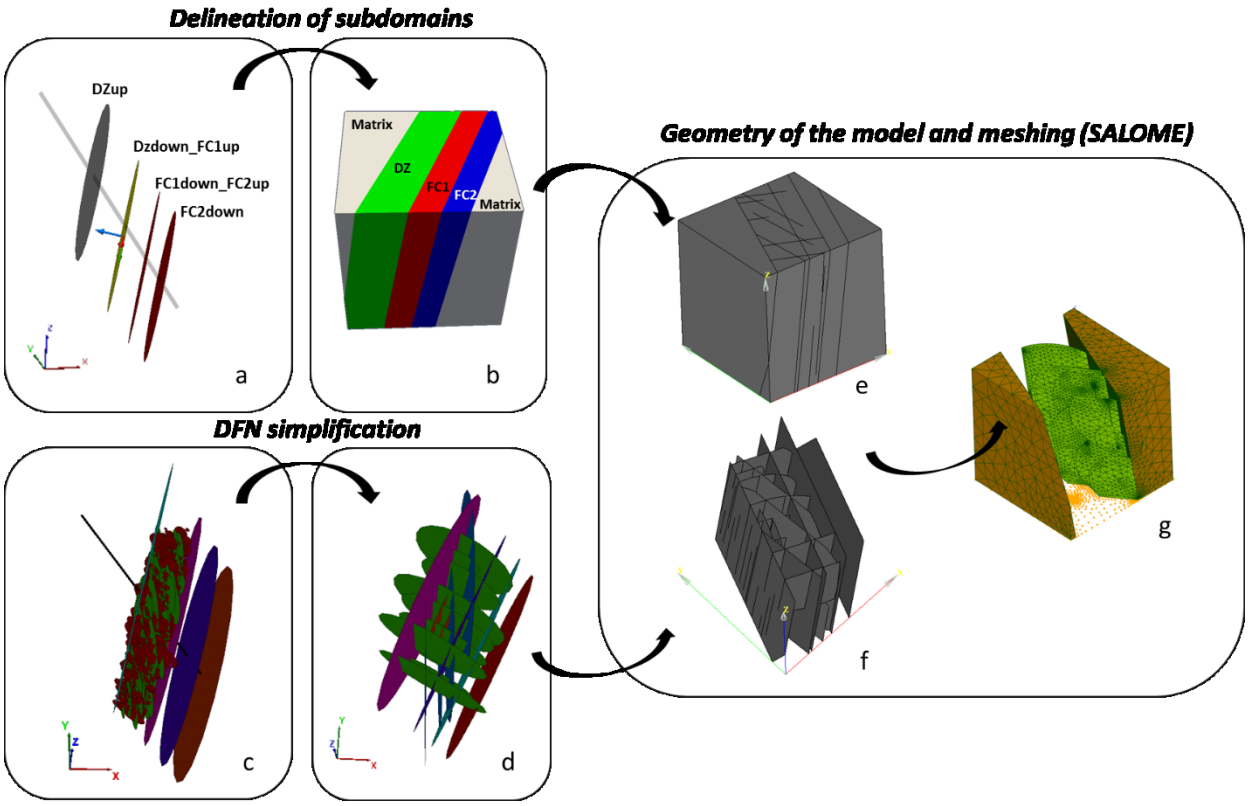

Figure 3. Main steps to build the geometry of the model

3.2 Hydraulic and thermal parameters

To carry out model computations, distributions of thermo-hydraulic properties (e.g., permeability, porosity, thermal conductivity, specific heat, etc.) for all the elements (fractures and porous media), and boundary conditions along the faces of the model are prescribed. During the development of the intial-state model for the fault zone reservoir considered, the formation properties (i.e. permeabilities of fractures) were varied in order to match the injectivity index and the main losses observed. Numerous simulations have been performed to match these constraints; in the following, we only present the final test that constitute the reference case of this study. The following Table 2 and Table 3 synthetize the values from this first step. The Figure 4 shows the permeability of the fractures, the permeability of the subdomains and the differential of pressure for the initial injection test (40 m^3/h during 12 hours). Note that the injectivity index obtained for the reference case is about 0.23 L/s/bar.

Table 2 Hydraulic parameters

Names of element	*Hydraulic parameters*	
Subdomains	**Permeability [m²]**	**Porosity**
Matrix	10^{-2}	0.15
DZ	10^{-21}	0.15
FC1	10^{-19}	0.15
FC2	10^{-14}	0.15
Fractures		
R (set)	2.08×10^{-14}	0.999
R2 (set)	8.33×10^{-16}	0.999
Fractures in FC1	10^{-19}	0.999
DZup	3.33×10^{-13}	0.999
Y (DZDown_FC1up, FC1down_FC2up, FC2down)	2.08×10^{-14}	0.999

Table 3 Thermal parameters

Names of element	*Thermal parameters*		
Solid	**Spe. Heat capacity [$J.kg^{-1}.K^{-1}$]**	**Thermal conductivity [$kg.m.s^{-3}.K^{-1}$]**	**Rock density [$kg.m^{-3}$]**
Matrix, DZ, FC1, FC2, Fractures	800	2.3	2650
Liquid			
Fluid	4200	0.6	f(T,P)

3.3 Initial and boundary conditions

As a first approximation, a hydraulic no-flow boundary condition is specified for the lateral (North, South, East, and West) and bottom model boundaries. For the top of the model, a Dirichlet boundary condition is applied (temperature and pressure). As mentioned

previously, a hydrostatic state is assumed for the reservoir, then the pressure is fixed in accordance with the depth of the top of the reservoir (-4062.46 m TVD). The initial temperature of the reservoir is constant around 200 °C and fixed at the top of the model.

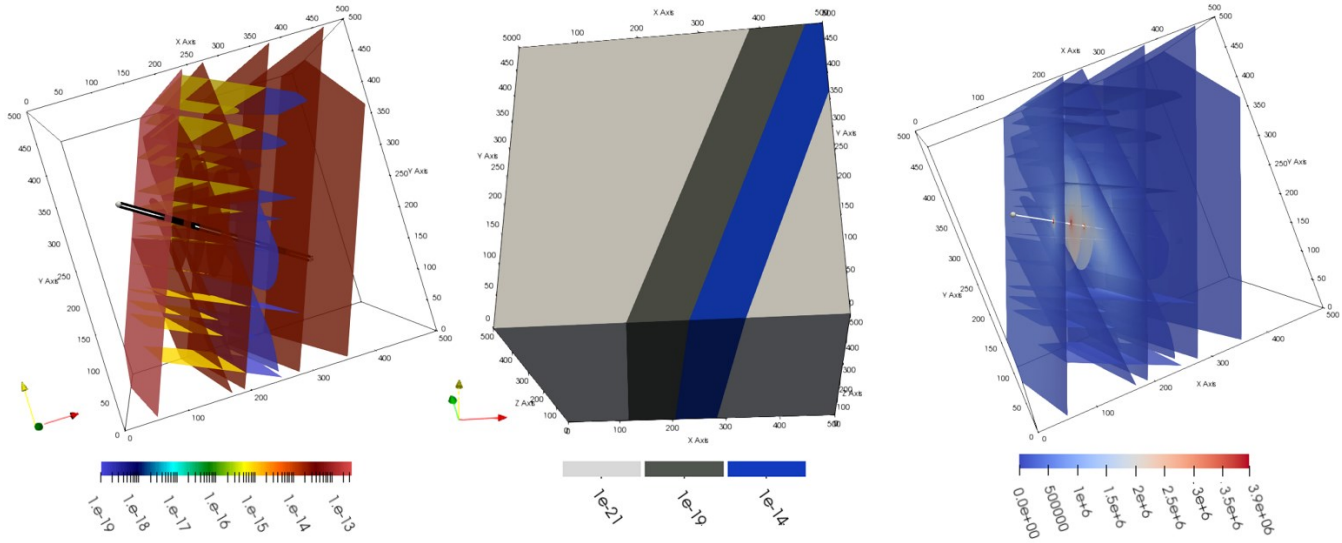

Figure 4. Initial model (reference); Left: Permeability of fractures (m²); Middle: Permeability of subdomains; Distribution of the differential of pressure (Pa) between initial state and after 12 h of injection

4. SIMULATIONS

The main idea of this work is to provide an overview of the impact of different stimulation methods considered to enhance the productivity of the targeted reservoir. The impact of the different technologies used to enhance the injectivity of the well such as stimulation methods (the hydraulic and thermal methods are considered) or such as multi-drain well geometries are studied. Here, we detailed the first results of this on-going work based on the results of companion papers (Blaisonneau et al., 2020; Peter-Borie et al., 2019). To assess the impact of each stimulation method, an injection test is performed (considering an injected fluid at a temperature of 50°C and a flow rate of 40 m^3/h during 12 hours). For each case, the injectivity index is calculated and then compared to others.

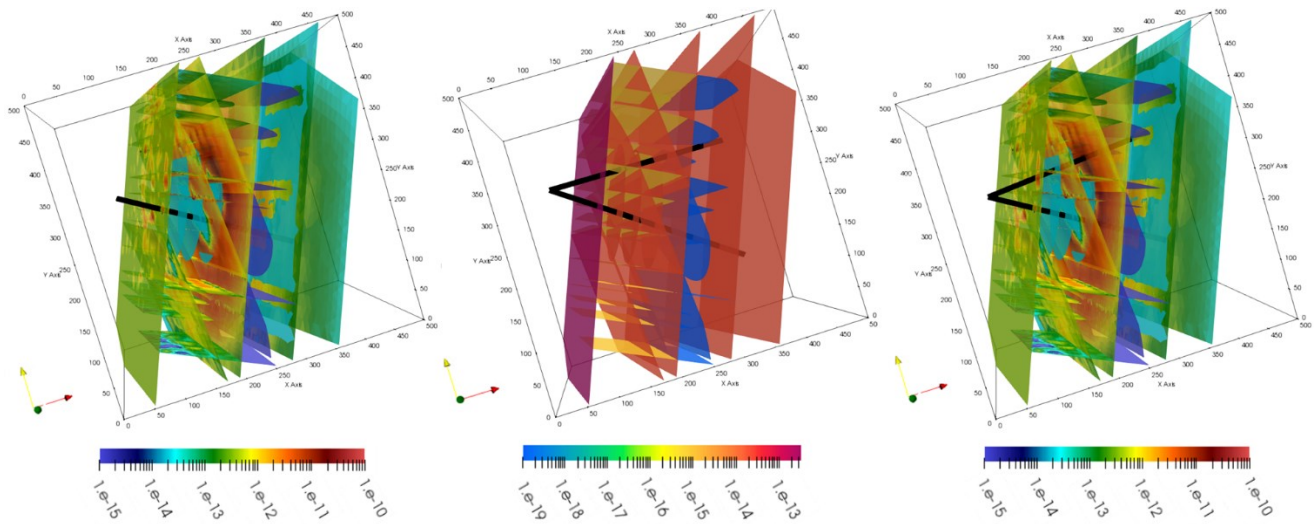

Figure 5. Permeability distribution for each model and well architecture. Left: Permeability resulting from hydraulic stimulation. Middle: Well architecture (two-legs). Right: Combined method: Hydraulic stimulation and well architecture are both deployed.

4.1 Hydraulic stimulation

In order to assess the injectivity gain by hydroshearing, hydro-mechanical numerical simulations are performed. The hydraulic stimulation is modelled as a multi-step fluid pressure increase. Modelling process details are available in the companion paper (Blaisonneau et al., 2020). The hydraulic aperture variations (considering the hydraulic criterion "irreversible residual apertures") resulting from the hydromechanical simulation (Blaisonneau et al., 2020) are imported into the hydrothermal model to modulate the initial reservoir properties in accordance with the hydraulic stimulation (Figure 5 left).

4.2 Well architecture

Multilateral well configurations are sophisticated well architectures developed to increase the well productivity/injectivity. A multilateral well consists of one primary well and one or more secondary wells issuing from the first (Aubert, 1998). The fault-zone

reservoir of Vendenheim seems to be a reasonable candidate for multilaterals configuration. The two-legs configuration is presented in the Figure 5 (middle and right). The performance of this well configuration is compared with a configuration with only one well (Figure 5 left). This well configuration is assessed in the reference case (initial permeability, before stimulation) and then in the case following the hydraulic stimulation in order to assess the combined effect on the injectivity.

4.3 Thermal stimulation

Thermal stimulation appears as a promising technique to enhance the productivity/injectivity of the reservoir. In line with the previous numerical simulations, the cooling of the reservoir will be different according to the stimulation methods applied and the well architecture implemented. Based on the combination of the results provided by the study of Peter-Borie et al., (2019) and the temperature field resulting from hydrothermal simulations (thermal field), the permeability variations (around the well and the matrix surrounding the fractures) will be implemented to assess the impact of thermal stimulation. Hereafter, we provide an example of the work carried out by Peter-Borie et al., (2019), which has been used to consider the impact of thermal stimulation. The Figure 6 demonstrates the permeability variations (around a fracture) resulting from a differential of temperature of 150°C (due to the injection of a cold fluid of 50°C). The fracture is at the center of the domain (y = 0, where the injection is considered) and the domain is subdivided in two subdomains (Figure 6). The upper part represents a granite and the bottom part a hydrothermalised granite sealed by quartz. After the injection of the cold fluid, thermal cracks have been created (Figure 6, left). The contours of cracks are delineated and the permeability of cracks calculated (Figure 6, middle). Then, an average permeability is estimated in Y-directions (Figure 6, right) according to this following relationship:

$$K_{avg} = \frac{\sum_{i=1}^{n} L_i}{\sum_{i=1}^{n} \left(\frac{L}{k}\right)_i} = \frac{1}{\sum_{i=1}^{n} \left(\frac{1}{k}\right)_i}$$

Where K_{avg} is the average permeability (m²), L_i the length of the subdomain i (m) in the Y-direction and k the permeability (m²) of the subdomain i.

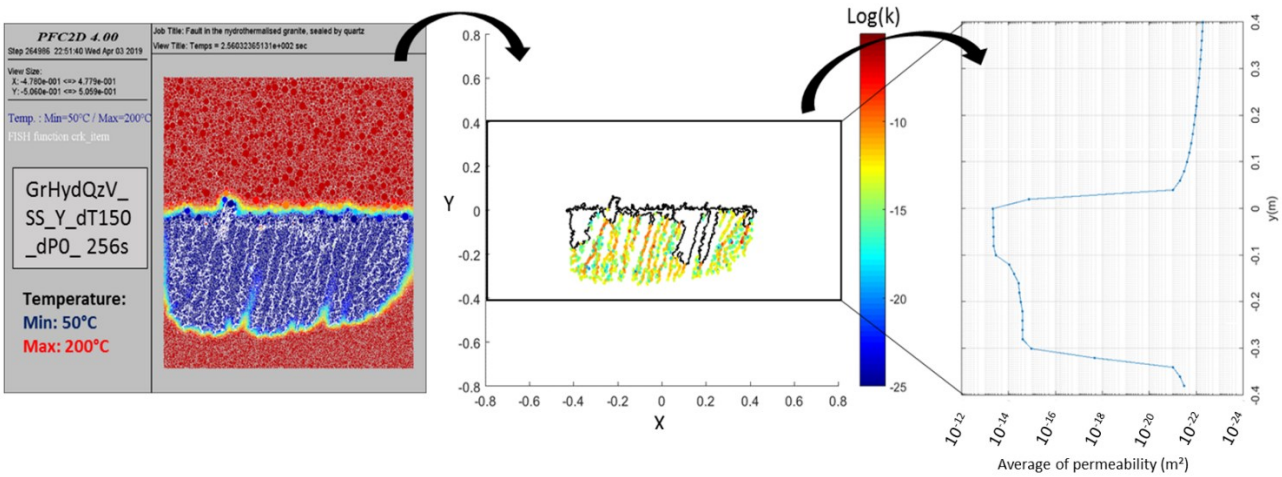

Figure 6. Left: Thermal cracks (and thermal field) in hydrothermalised granite sealed by quartz (bottom part) and granite (upper part). In the middle: Contours and permeability of thermal cracks. On the right, average permeability estimated around the fracture.

Based on these results, we can notice that for a short lapse of time and a temperature difference of 150°C in a hydrothermalised granite, the permeability reached a value around 5×10^{-13} m² close to the fracture. This contrasts sharply with the granite (upper part) where the permeability is slightly modified very close to the fracture. Note that this study has been carried out for different kinds of granites, as well as different temperature contrasts and also for different configurations, such as around the well providing a set of values of permeability variations that can be used to assess the impact of thermal stimulation. As a first approximation, a simulation considering an injection test of a fluid at 50°C (40 m³/h during 30 days) is performed. The resulting thermal field (differential of temperature, see Figure 7, left) is used to identify zones impacted by thermal cracks and then in order to implement the permeability variations in accordance with these zones (see Figure 7, right). Then, the new permeability field is used to assess the impact of thermal stimulation using the same injection test (40 m³/h during 5 days) as for previous simulations.

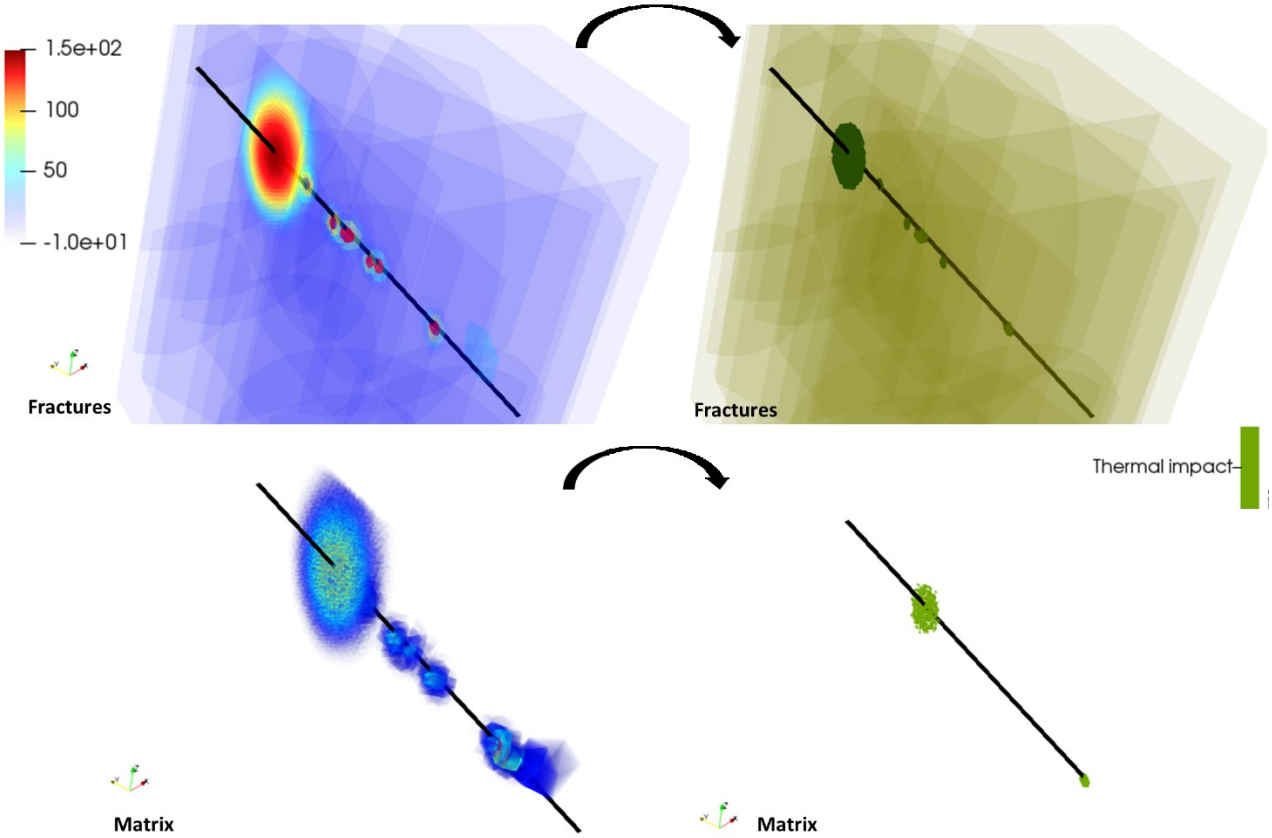

Figure 7. Left: Differential of temperature (between initial and last step: 30 days). Right: the resulting zones impacted by thermal cracks on the fractures and within the matrix.

4.4 Results

The different methods and their combined impacts are compared in terms of injectivity (Figure 8). Firstly, we can describe the respective impact of each method (hydraulic stimulation, thermal stimulation and well architecture) in comparison with the initial state of the reservoir. For the hydraulic stimulation (HM), the injectivity index is multiplied by 1.5. As well, in this particular case and for the specific well architecture tested (two-legs) the injectivity index is multiplied by a factor of 1.4. The impact of the thermal stimulation is slightly inferior, with the injectivity multiplied by 1.2. Based on these first results, it seems that these methods are almost equivalent to enhance the initial productivity of the targeted reservoir (even if these specific results show a slight difference between these methods in favour of the hydraulic stimulation). However, the HM results are highly dependent on the mechanical parameters implemented into the hydromechanical model, which require further analysis (assessment of the mechanical parameters, see Blaisonneau et al., 2020a). The main difference between these methods can be assessed through the pressure and temperature differentials (Figure 9 and Figure 10). In comparison with the reference case, the impact of the TM stimulation (Figure 9, TM) is localized within the first main fracture, which results from the main zone impacted by thermal cracks (Figure 7). The results of the HM stimulation (Figure 9, HM) is clearly different: the pressure differential is very localized and lower due to higher permeability of some fractures which were almost impermeable and, therefore, result in a better distribution of the pressure within the reservoir. Then, more fractures are permeable and the temperature differential is reduced (Figure 10, HM). The "two-legs" architecture increases the number of points to distribute the injection and then results in a better injectivity. However, the envelope of the pressure differential is comparable to the reference case (Figure 9, Two-legs).

Then, simulations were performed to study the combined impact of these respective methods (scenarios). The results of scenarios are summarised in Figure 8 (injectivity). Overall, the combined impact of methods allows an increase in injectivity. The successive effect of the hydraulic stimulation and the well architecture would appear highly beneficial to the reservoir injectivity. In comparison with the reference case, the injectivity index is multiplied by a factor of 2.6. The combined impact of the TM stimulation seems relevant in all cases, except for the case (HM + 2 legs + TM) where the TM stimulation can be slightly negative. In that specific case, the permeability variations (around the well and the matrix surrounding the fractures in accordance with the differential of temperature) is related to the quantity of cold water injected into the reservoir. An increase of the flowrate (or a longer duration) could be considered due to the better injectivity after the first two methods, then the zones impacted by thermal cracks will be greater and thus the injectivity index could be greater. This latter finding requires further investigation.

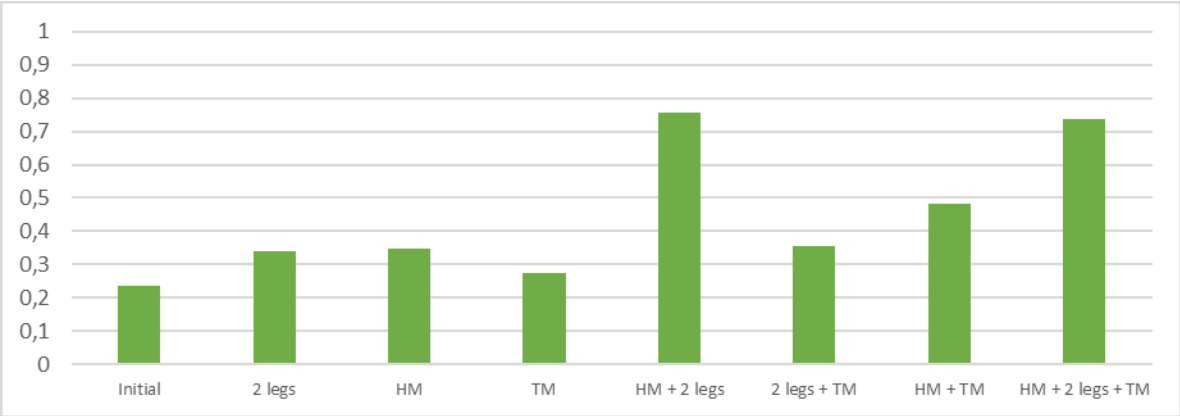

Figure 8. Injectivity (L/s/bar) for each case

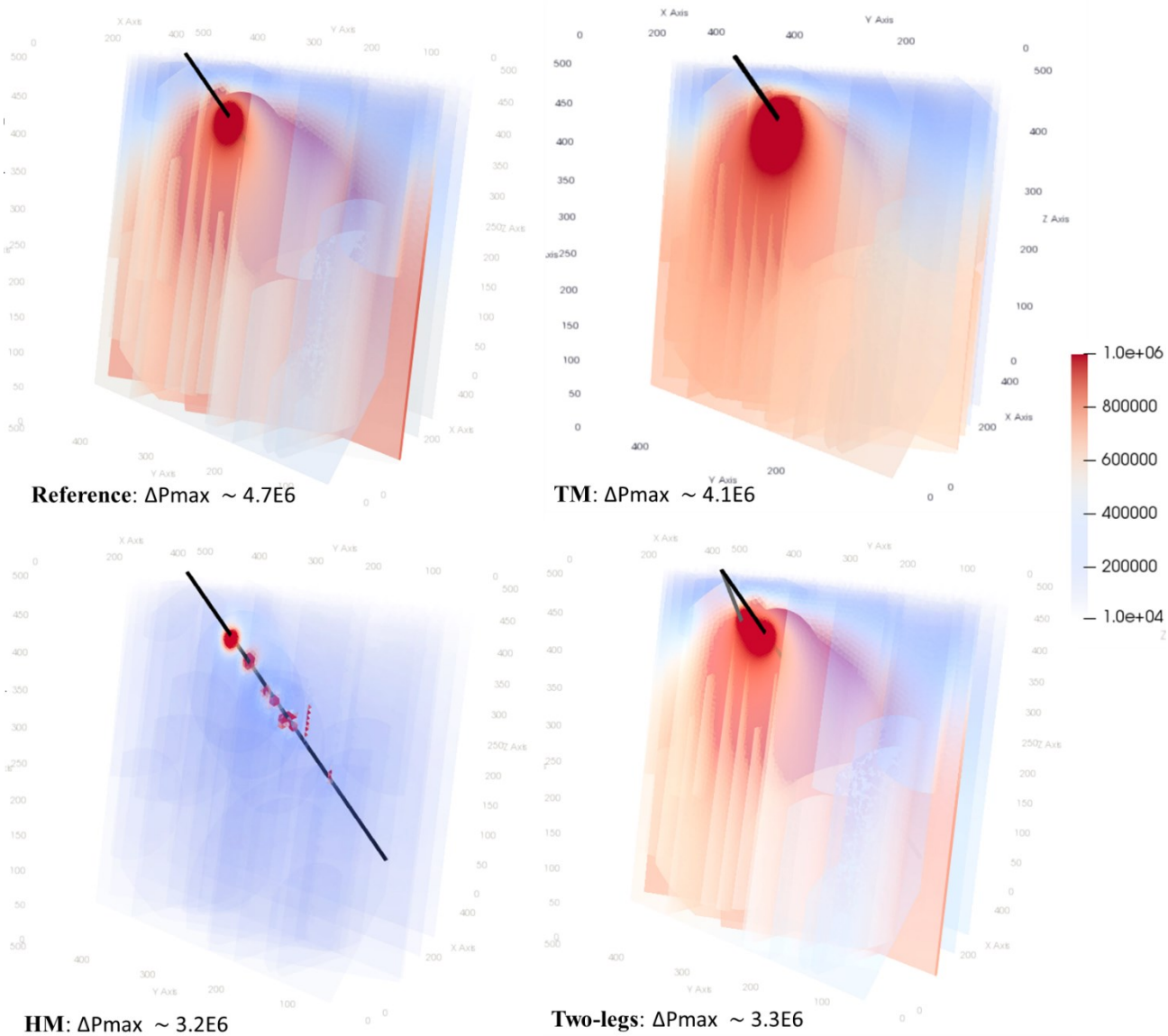

Figure 9. Differential of pressure for the different tested cases (injection flowrate of 40 m^3/h during 5 days)

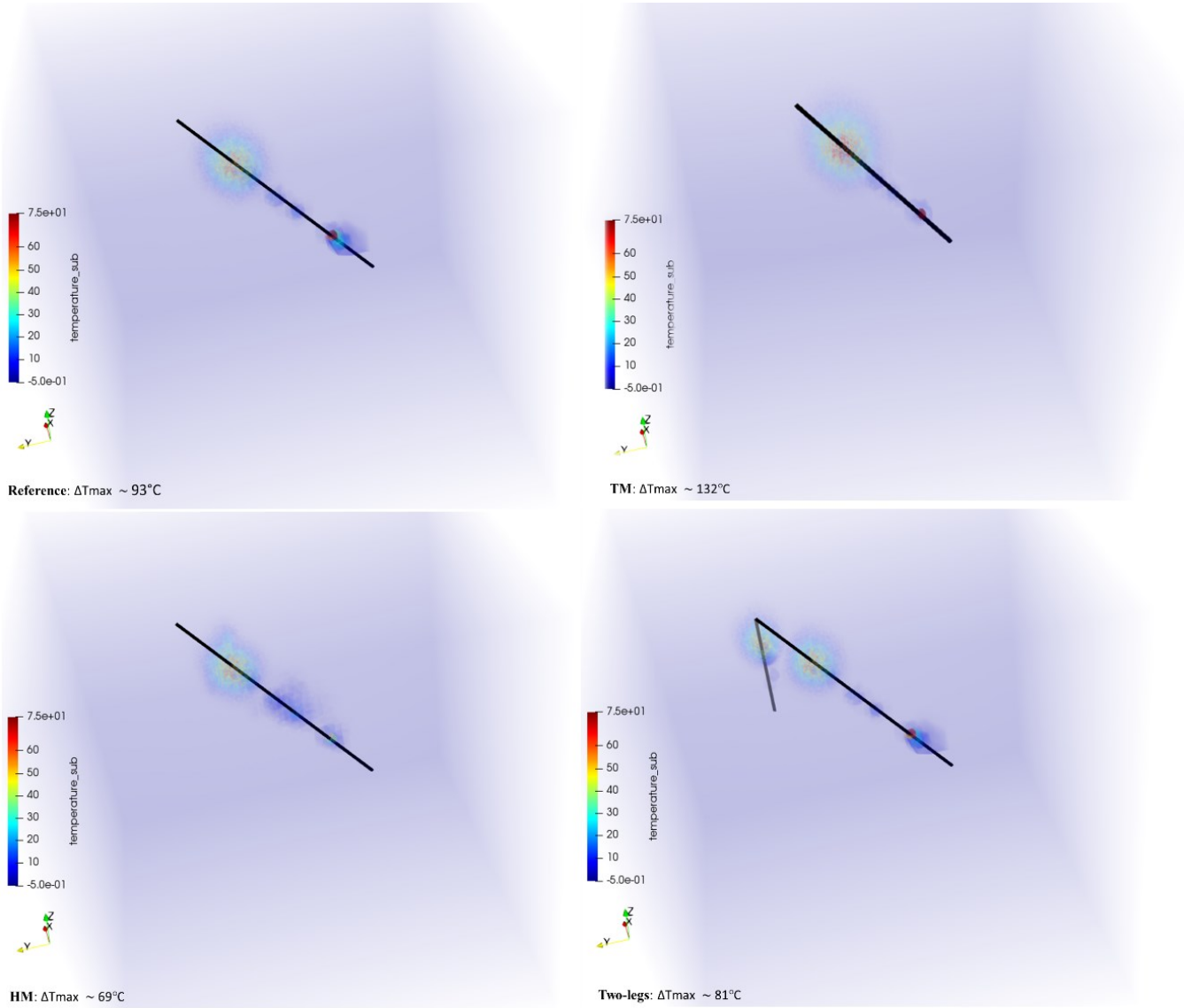

Figure 10. Temperature field (differential of temperature °C in the matrix surrounding the fractures after 5days) around the well for each case

5. CONCLUSION

The aim of this paper is to provide an overview of a study carried out in the framework of the H2020-DEEPEGS project. In this paper, we propose to investigate the impact of well architecture for a fault zone geothermal reservoir using a hydrothermal model based on a hybrid approach (including a DFN). The hydrothermal model developed for this specific demonstrator is used to study the impact of hydraulic stimulation (HM) (based on the results provided by the hydromechanical study, Blaisonneau et al., 2020) and the impact of the well architecture. Then, this hydrothermal model is also used to test the impact of the permeability variations resulting from the thermo-mechanical numerical modeling (Peter-Borie et al., 2019), which results from the "cold" water injection and the associated thermal cracks is also implemented in order to assess the impact of thermal stimulation. The impact of each method is assessed through the increase of the injectivity accoding to pressure differential as well as the resulting thermal field. For the case study considered here, it appears that the different methods investigated (HM, TM, two-branches architecture) lead to the same order of magnitude in terms of injectivity improvement. The injectivity for each method considered separately is multiplied by a factor comprised between 1.2 and 1.5. The combination of methods (HM + two-legs) enables further improvement of injectivity, with multiplication factor around 2.6. It should be kept in mind that results are very dependent from the choice of parameters an should thus be considered cautiously.. The last step of this study will be to implement the effect of the chemical stimulation (acid injection) and test the impact of different scenarios (successive stimulation methods) based on the presented work. The import of constraints provided by other numerical codes into this unique hydrothermal model offers a way to test different scenarios of stimulation in order to identify the most appropriate solution as well as to better understand the mechanisms related to each stimulation methods.

ACKNOWLEDGMENTS

This study was part of the DEEPEGS project, which received funding from the European Union HORIZON 2020 research and innovation program under Grant agreement no. 690771.

REFERENCES

Aubert, W.G., 1998. Variations in Multilateral Well Design and Execution in the Prudhoe Bay Unit, in: IADC/SPE Drilling Conference,3-6 March,Dallas, Texas. Society of Petroleum Engineers.

Baujard, C., Genter, A., Dalmais, E., Maurer, V., Hehn, R., Rosillette, R., Vidal, J., Schmittbuhl, J., 2017. Hydrothermal characterization of wells GRT-1 and GRT-2 in Rittershoffen, France: Implications on the understanding of natural flow systems in the rhine graben. Geothermics 65, 255–268. https://doi.org/10.1016/j.geothermics.2016.11.001

Beaude, Laurence, Beltzung, T., Brenner, K., Lopez, S., Masson, R., Smai, F.F., Thebault, J.-F.F., Xing, F.F., 2017a. Parallel geothermal numerical model with faults and multi-branch wells. ESAIM Proc. Surv. in press.

Beaude, L., Brenner, K., Lopez, S., Masson, R., Smai, F., 2018. Numerical Modeling of High Energy Geothermal Systems with Soil Atmosphere Boundary, in: 43rd Workshop on Geothermal Reservoir Engineering. Stanford, California, pp. 1–12.

Beaude, L., Brenner, K., Lopez, S., Masson, R., Smai, F., 2017. Non-isothermal Compositional Two-Phase Darcy Flow: Formulation and Outflow Boundary Condition., in: Springer, Cham (Ed.), Springer Proceedings in Mathematics and Statistics. pp. 317–325.

Beaude, Laurence, Brenner, K., Lopez, S., Masson, R., Smai, F., 2017b. Non-isothermal Compositional Two-Phase Darcy Flow: Formulation and Outflow Boundary Condition, in: Springer Proceedings in Mathematics and Statistics. Springer, Cham, pp. 317–325. https://doi.org/10.1007/978-3-319-57394-6_34

Blaisonneau, A., Maury, J., Armandine Les Landes, A., Guillon, T., 2020. Hydromechanical modelling of the hydraulic stimulation of a fault zone as deep geothermal target, in: World Geothermal Congress 2020. Reykjavik, Iceland.

Chen, Z., Zhang, Y., 2009. Well flow models for various numerical methods. Int. J. Numer. Anal. Model. 6, 375–388.

Cloos, H., 1928. Experimenten zur inneren Tektonic, Centralblatt fur Mineralogie und Paleontologie.

Coats, K.H.H., 1989. Implicit Compositional Simulation of Single-Porosity and Dual-Porosity Reservoirs. SPE Symp. Reserv. Simul. https://doi.org/10.2118/18427-MS

Cruz Mermy, D., Dezayes, C., Durst, P., Guignat, S., Martin, P., 2012. Evaluation des potentiels géothermiques profonds de la Communauté urbaine de Strasbourg. Orléans.

Edel, J.-B., Schulmann, K., Rotstein, Y., 2007. The Variscan tectonic inheritance of the Upper Rhine Graben: evidence of reactivations in the Lias, Late Eocene–Oligocene up to the recent. Int. J. Earth Sci. 96, 305–325. https://doi.org/10.1007/s00531-006-0092-8

Eymard, R., Guichard, C., Herbin, R., Masson, R., 2012. Vertex-centred discretization of multiphase compositional Darcy flows on general meshes. Comput. Geosci. 16, 987–1005. https://doi.org/10.1007/s10596-012-9299-x

Gentier, S., Rachez, X., Peter-borie, M., Loubaud, M., 2014. A flow model of the deep geothermal reservoir of Soultz-sous-Forêts (France), in: ARMA American Rock Mechanics Association 13-279. San Francisco.

Glaas, C., Genter, A., Girard, J.F., Patrier, P., Vidal, J., 2018. How do the geological and geophysical signatures of permeable fractures in granitic basement evolve after long periods of natural circulation ? Insights from the Rittershoffen geothermal wells (France). Geotherm. Energy 6. https://doi.org/10.1186/s40517-018-0100-9

Katz, Y., Weinberger, R., Aydin, A., 2004. Geometry and kinematic evolution of Riedel shear structures, Capitol Reef National Park, Utah. J. Struct. Geol. 26, 491–501. https://doi.org/10.1016/j.jsg.2003.08.003

Lopez, S., Masson, R., Beaude, L., Birgle, N., Brenner, K., Kern, M., Smai, F., Feng, Xing, F., 2018. Geothermal Modeling in Complex Geological Systems with the ComPASS Code, in: 43rd Workshop on Geothermal Reservoir Engineering. Stanford University, Stanford, California,.

Peaceman, D.W., 1983. Interpretation of well-block pressures in numerical reservoir simulation with nonspace grid blocks and anisotropic permeability. Soc. Pet. Eng. 23(3).

Peaceman, D.W., 1978. Interpretation of Well-Block Pressures in Numerical Reservoir Simulation. Soc. Pet. Eng. J. 18, 183–194. https://doi.org/10.2118/6893-PA

Peter-Borie, M., Loschetter, A., Blaisonneau, A., Tran, V.H., Gaucher, E., Sigurdsson, O., Gudmundur Omar, F., Damy, P.-C., Le Lous, M., Tulinius, H., 2019. Thermal stimulation of the deep geothermal wells: insights from the H2020-DEEPEGS project, in: European Geothermal Congress 2019. Den Haag, The Netherlands.

Peter-borie, M., Loschetter, A., Maury, J., Team, and D., 2020. Assessment of Geothermal Well Productivity Improvement Technologies: an Overview from the DEEPEGS Project, in: World Geothermal Congress 2020. Reykjavik, Iceland.

Ribés, A. (EDF R., Bruneton, A. (CEA), Geay, A. (EDF), 2017. SALOME : an Open-Source simulation platform integrating ParaView SALOME. https://doi.org/10.13140/RG.2.2.12107.08485

Riedel, W., 1929. Zur Mechanik Geologischer Brucherscheinungen.

Schumacher, M.E., 2002. Upper Rhine Graben: Role of preexisting structures during rift evolution. Tectonics 21, 6-1-6–17. https://doi.org/10.1029/2001TC900022

Xing, F., Masson, R., Lopez, S., 2017. Parallel numerical modeling of hybrid-dimensional compositional non-isothermal Darcy flows in fractured porous media. J. Comput. Phys. 345, 637–664. https://doi.org/10.1016/j.jcp.2017.05.043

Ziegler, P.A., 1990. Geological atlas of Western and Central Europe, in: Mesozoic and Cenozoic.